Chapter 2
Inertial Migration of Cancer Cells in a Microfluidic Device

Tatsuya Tanaka, Takuji Ishikawa, Keiko Numayama-Tsuruta, Yohsuke Imai, Hironori Ueno, Takefumi Yoshimoto, Noriaki Matsuki, and Takami Yamaguchi

Abstract The circulating tumor cell (CTC) test is used to evaluate the condition of breast cancer patients by counting the number of cancer cells in peripheral blood samples. Although microfluidic systems to detect or separate cells using the inertial migration effect may be applied to this test, the hydrodynamic forces acting on cancer cells are incompletely understood. In this chapter, we explain the inertial migration of cancer cells in microchannels. We also explain fabrication techniques of microchannels used in the experiments. By measuring the cell migration probability, we examined the effects of cell deformability and variations in cell size on the inertial migration of cancer cells. The results clearly illustrate that cancer cells can migrate towards equilibrium positions in the similar manner with rigid spheres. These results will be important for the design of microfluidic devices for the CTC test.

T. Tanaka (✉) • T. Ishikawa • Y. Imai • T. Yoshimoto
School of Engineering, Tohoku University, 6-6-01 Aoba, Sendai 980-8579, Japan
e-mail: tatsuya@pfsl.mech.tohoku.ac.jp

K. Numayama-Tsuruta • T. Yamaguchi
School of Biomedical Engineering, Tohoku University, 6-6-01 Aoba, Sendai 980-8579, Japan

H. Ueno
International Advanced Research and Education Organization, Tohoku University, 6-6-01 Aoba, Sendai 980-8579, Japan

N. Matsuki
Department of Biomedical Engineering, Okayama University of Science, 1-1 Ridai-cho, Okayama 700-0005, Japan

M.W. Collins and C.S. König (eds.), *Micro and Nano Flow Systems for Bioanalysis*, Bioanalysis 2, DOI 10.1007/978-1-4614-4376-6_2,

2.1 Introduction

The incidence of breast cancer is increasing in many developed countries. In its diagnosis, it is crucial to detect metastasis or cancer recurrence at an early stage. The circulating tumor cell (CTC) test has been widely adopted for evaluating the prognosis of breast cancer [3,6,7]. In this test a patient's condition is assessed by counting the number of cancer cells in a peripheral blood sample. For this purpose, it is necessary to distinguish cancer cells from other blood cells, and the accuracy of the CTC test is strongly dependent on the precision of cell identification.

Microfluidic devices for cell separation have received much attention. These devices can be classified into two groups based on whether the method of separation is active or passive [2]. While in active separation an external field is involved, such as would be caused by magnetic or electric means, in passive separation an external force is not needed. Passive separation devices have a number of advantages compared with active separation alternatives; these include miniaturization, inexpensive production cost, and easy handling of the device. Examples of passive cell separation methods are the pillar structures method [18,21], hydrodynamic filtration [23,24], and biomimetic separation [11,19]. However, despite their high separation efficiency, devices using such methods are unsuitable for the CTC test because of their low throughput. To overcome this difficulty, a passive cell separation method has been investigated which involves inertial migration.

Segre and Silbergerg [17] originally described the inertial migration process in 1962. When the Reynolds number of a particle is not too small, the inertial force on it generates a drift velocity perpendicular to the streamline. Hence, a group of particles flowing in a channel will move towards the sidewalls, and eventually the particles will be aligned passively at specific positions. Microfluidic devices using inertial migration have been proposed for separating various rigid particles [1,5,16]. The throughput of this method is very high, because the inertial effect becomes significant only at high velocities. The time required for particle separation is often much shorter than that of other methods, and forms its major advantage.

Recently, some groups have succeeded in applying the inertial migration effect to the detection or separation of different types of living cells. Kuntaegowadanahalli et al. [12] developed a five-loop Archimedean spiral microchannel and separated SH-SY5Y neuroblastoma cells (~15 μm in diameter) from C6 rat glioma cells (~6 μm in diameter) in a dilute cell suspension (volume fraction, ~0.05%). In addition to inertial migration forces, their microfluidic device used the Dean force generated by the centrifugal effect. The separation efficiency exceeded 80%, with a high throughput of 1×10^6 cells/min. Hur et al. [9] demonstrated how cells flowing through channels could be aligned three-dimensionally via the inertial migration effect. As they focused on cells at a specific depth, the effects of cell overlap and out-of-focus motion were ignored. Their device allowed red blood cells and leukocytes to be counted with high sensitivity via image analysis. Using a similar approach to Kuntaegowadanahalli et al. [12], Carlo et al. [4] applied the inertial

force effect to isolate platelets from other blood cells in a dilute suspension, enriching the relative number of platelets by 100-fold. These examples illustrate the potential of applying inertial migration to the development of a microfluidic device for the CTC test.

If cancer cells could be separated from blood cells using the inertial migration effect, this would facilitate the development of a microfluidic device for the CTC test. To this end, we have recently studied the inertial migration of cancer cells in a straight microchannel [22], which is introduced in this chapter. In Sect. 2.2, we briefly explain the basic mechanism of inertial migration. Section 2.3 describes the fabrication of a polydimethylsiloxane (PDMS) microchannel, for the sake of readers who are not familiar with microfluidics. We explain the preparation of cancer cells in Sect. 2.4, particularly for readers who have no experience of cell culturing. Section 2.5 gives the results of initial experiments using rigid spheres: these enable the efficiency of inertial migration to be demonstrated. Section 2.6 presents experimental results using cancer cells, thus showing how inertial migration may be applied to them. The results given in Sects. 2.5 and 2.6 are mainly from Tanaka et al. [22], and further details such as the effects of red blood cells on the migration of cancer cells can be found in that paper. This chapter focuses on the fundamental principles of the inertial migration of cancer cells in a microchannel.

2.2 Mechanism of Inertial Migration

Figure 2.1a shows the principles governing the inertial migration of particles flowing in a tube. The particles are subject to drag and inertial lift forces. The drag force (F_D) drives particles along their streamlines, while the shear-induced inertial lift force (F_{IL}) drives them away from the channel center and toward the sidewalls. The particle Reynolds number (Re_p) is a key factor in inertial migration, being defined as $\mathrm{Re_p} = \rho d^2 \dot{\gamma}/\mu$, where d is the diameter of a particle, $\dot{\gamma}$ the shear rate, and ρ and μ the density and viscosity respectively. It represents the ratio of the inertial force to the viscous force acting on the particles. When $Re_p \ll 1$, inertial migration does not occur, and the particles follow the streamlines. When Re_p is not negligibly small, inertial force acts on the particles, and they tend to drift from the streamlines. When particles come close to the wall, the wall-induced inertial lift force (F_{WL}) appears in addition to F_{IL}. These two forces act in opposite directions, and the particles tend to migrate towards equilibrium positions, where the magnitudes of the two inertial forces are balanced.

These equilibrium positions depend mainly on the channel geometry and Re_p (Fig. 2.1b). In a cylindrical channel with moderate Re_p, particles align in an annulus at a radius of about $0.6R$, where R is the channel wall radius [17]. The radius of the equilibrium annulus increases with increasing Re_p because of the increase in F_{IL} [14,15]. For a channel with a square cross-section, particles tend to align near the wall, and the equilibrium positions form the sides of a small square (cf. Fig. 2.1b). For a channel with a rectangular cross-section, the equilibrium positions are near

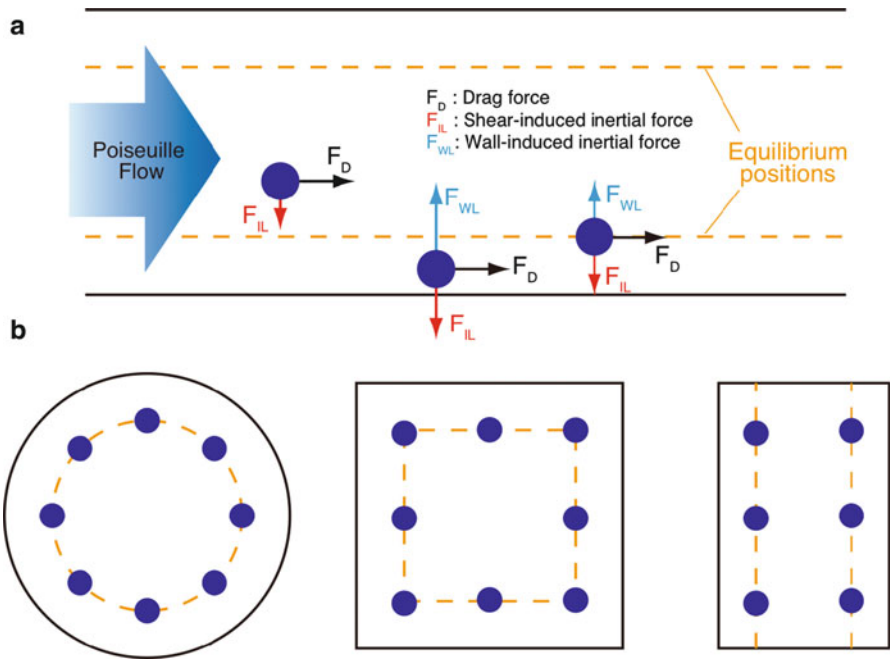

Fig. 2.1 The principle of the inertial migration of particles: (**a**) mechanism of the migration of particles toward their equilibrium positions and (**b**) the equilibrium positions in different channel geometries

the walls of the longer sides [1], because a greater shear rate acts on the particles along the narrower dimension. In terms of particle separation, a rectangular channel is preferable because the number of equilibrium positions is reduced and it is easier to guide particles toward a collecting outlet in a microfluidics device.

The migration length (L_m), i.e., the channel length required for the migration of rigid spheres, is obtained by considering the balance of forces between the shear-induced migration force and the viscous drag force. Bhagat et al. [1] derived L_m as

$$L_m = \frac{3\pi\mu}{2\rho U}\left(\frac{W}{a}\right)^3, \tag{2.1}$$

where U is the average velocity in the channel, W the half-width of the channel, and a the radius of a rigid sphere. When the channel length is much larger than L_m, most of the particles migrate to equilibrium positions. Consequently, L_m is one of the most important parameters in the design of a microchannel for particle separation. In Sect. 2.5, we show that (2.1) is a good approximation for describing the migration of rigid spheres. In Sect. 2.6, we show that (2.1) does not precisely predict the migration of cancer cells, as the L_m for cancer cells is longer than the value for rigid spheres.

2.3 Fabrication of a Polydimethylsiloxane Microchannel

A standard soft lithography technique is widely used for fabricating microchannels such as those with a stenosis [8] or with a bifurcation and confluence [10]. Here, as an example, we outline the fabrication procedure using photoresist SU-8 and polydimethylsiloxane (PDMS). SU-8, an epoxy-based photoresist, is widely used for fabricating channel molds. It can sustain structures with high aspect ratios, so that vertical sidewalls can be built easily. PDMS is a polymeric silicone with excellent material properties for making microfluidic devices. Its good optical transparency, good biocompatibility, accurate replication of fine and complex geometries, high thermal stability, and low cost make PDMS one of the most popular materials for microfluidic devices.

Figure 2.2 is a schematic of the procedure used for fabricating the microchannel. First (Step 1, Fig. 2.2) to enhance the adhesiveness of the photoresist on the wafer, the surface of a silicon wafer was cleaned using piranha solution, which is a mixture of sulfuric acid and hydrogen peroxide, to remove organic residues. After the substrate was washed with deionized water to remove all traces of the cleaning solution, the photoresist (SU-8 2075; Kayaku MicroChem, Tokyo, Japan) was applied to the silicon wafer with a spin coater. The thickness of the photoresist was controlled by adjusting the revolving speed of the spin coater (Step 2). Then, the wafer was glued to a photomask on which the channel geometry had been drawn. Finally, the wafer was exposed to ultraviolet light (Step 3) completing the silicon mold with the microchannel pattern (Step 4).

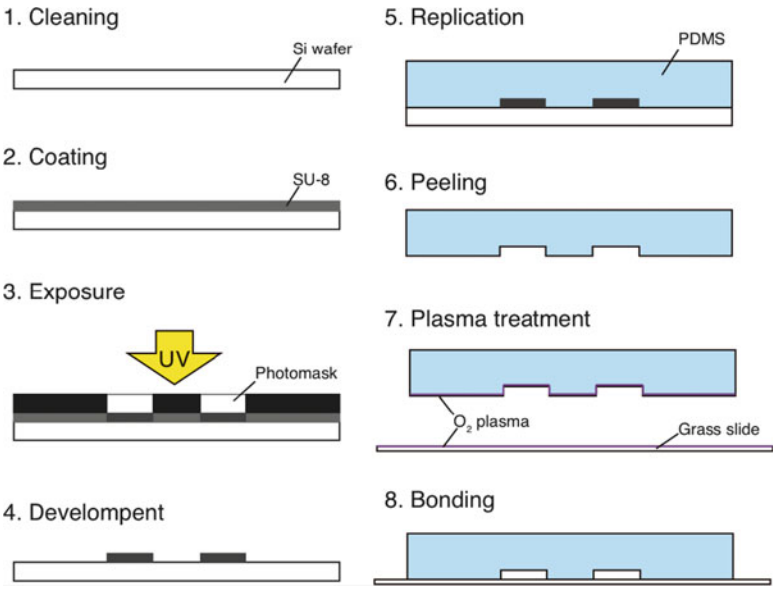

Fig. 2.2 Procedure for fabricating a PDMS microchannel

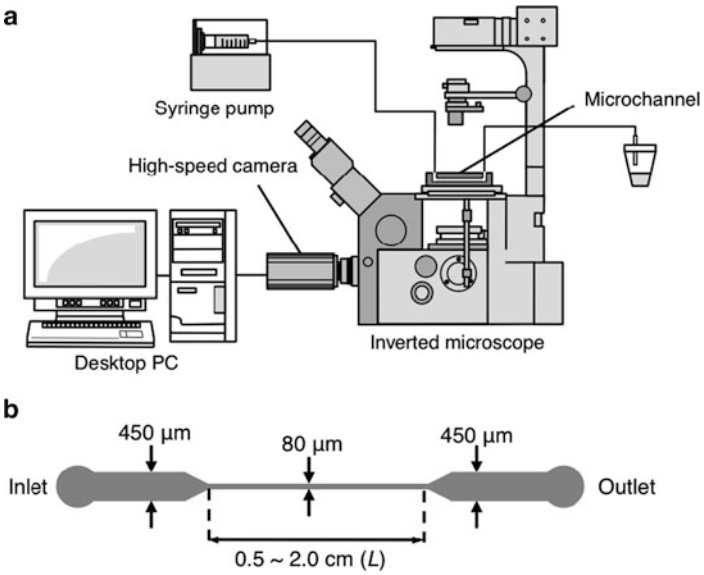

Fig. 2.3 Experimental setup: (**a**) schematic representation of the experimental setup; and (**b**) Geometry of PDMS microchannel. The height of the channel is 220 µm [22]

PDMS (Silpot 184; Dow Corning, Midland, MI) was prepared (Step 5) by mixing the base compound and curing agent at a weight ratio of 10:1. After removing the bubbles created during mixing, the mixture was poured on the master mold and cured by baking for about 40 min at 85°C. The PDMS was peeled (Step 6) from the master, and the fluidic ports used as the inlets and outlets of the fluidic device were created using a biopsy punch (Kai Industries, Gifu, Japan). For channels with very fine patterns, it is sometimes difficult to peel the PDMS channel from the master mold. In such cases, mold release agents are useful. Finally, to prevent fluid leakage from the gap between the PDMS and glass slide, an oxygen plasma treatment was applied (Step 7) to irreversibly bind (Step 8) the PDMS to the glass. Each step is straightforward, although special facilities are necessary, including a clean room and photolithography equipment. Alternatively, a private company may be contracted to fabricate the PDMS microchannel. In Sects. 2.5 and 2.6, we use a simple microchannel (cf. Fig. 2.3b) made using this technique.

2.4 Cell Preparation and Working Fluids

This section explains the preparation of cells and sample fluids used to perform the experiments in Sects. 2.5 and 2.6. The poorly differentiated human breast cancer cell line MDA-MB-231 was used. The cells in RPMI 1640 (Invitrogen,

Carlsbad, CA) with 10% fetal bovine serum (Thermo Fisher Scientific, Waltham, MA) and 1× antibiotic–antimycotic solution (Invitrogen) were cultured in 25-cm^2 tissue culture flasks at 37°C under 5% CO_2 (cf. [10]). For the experiments, cells were grown to 80–90% confluence, dissociated by the addition of 0.25% trypsin–EDTA (Invitrogen), harvested, and washed twice with Dulbecco's phosphate-buffered saline (PBS; Invitrogen).

Two different fluid samples were used in Sects. 2.5 and 2.6, respectively: a dilute suspension of 15-μm-diameter rigid spheres (FluoSpheres polystyrene microspheres; Invitrogen) in PBS and a dilute suspension of cancer cells (MDA-MB-231) in PBS. The concentrations of the rigid spheres and cancer cells were about 1×10^5 particles or cancer cells per milliliter. The density and viscosity at 25°C were 1.05×10^3 kg/m^3 and 1.15×10^{-3} Pa s, respectively.

2.5 Inertial Migration of Rigid Spheres in a Microchannel

The experimental setup for studying the inertial migration of rigid spheres is shown in Fig. 2.3a. The experimental apparatus consisted of an inverted microscope (IX71; Olympus, Tokyo, Japan) and a high-speed camera (Phantom v7.1; Vision Research, Wayne, NJ). A microchannel was placed on the stage, and the sample was injected using a syringe pump (IC 3101; KI Scientific, Holliston, MA). Images of the rigid spheres, taken with the high-speed camera, were recorded on a desktop computer.

A schematic of the PDMS microchannel is shown in Fig. 2.3b. A strong inertial force was induced on the particles flowing in the narrow test section, where Re_p was large. The test section of the channel was 80 μm wide, 220 μm high, and 1.0 cm long. To facilitate image analysis, the width of the microchannel was increased to 450 μm upstream and downstream from the test section.

The behavior of rigid spheres was observed upstream and downstream from the test section. A syringe pump was used to control the flow rate within the range 64-256 μL/min, corresponding to a Re_p of 0.16–0.62. To analyze particle behavior, the probability density of the width position from the center was calculated using the following equation:

$$P_i = \left(\sum_{j=1}^{M} n_{i,j} \right) \Bigg/ \left(\sum_{j=1}^{M} \sum_{i=1}^{N} n_{i,j} \right) \tag{2.2}$$

where P_i is the probability density at section i, M is the total number of frames recorded at 40-ms intervals, and $n_{i,j}$ is the number of particles in section i at frame j. The half-width of the channel was split into 50 sections (i.e., $n = 50$), and each was 4.5 μm wide. To calculate the probability density, at least 100 particles were counted in each experiment.

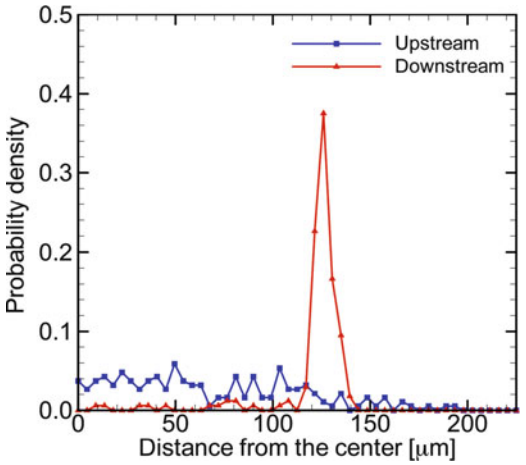

Fig. 2.4 Probability density of the width position of rigid spheres at the upstream and the downstream of the test section with $Re_p = 0.622$. The sidewall is located 225 μm from the center [22]

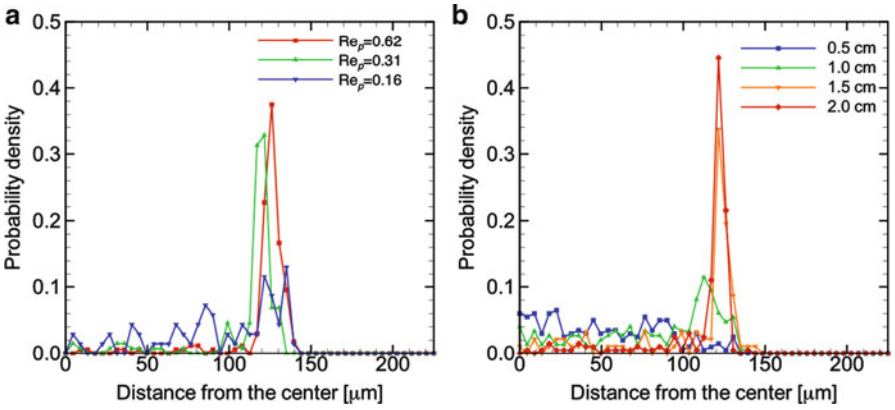

Fig. 2.5 Probability density of the width position of rigid spheres at the downstream of the test section: (**a**) effect of particle Reynolds number Re_p ($L = 1.0$ cm); and (**b**) effect of the channel length L ($Re_p = 0.16$) [22]

Figure 2.4 shows the probability density of the width position of rigid spheres upstream and downstream, with $Re_p = 0.62$. The probability density upstream was relatively uniform, while that downstream peaked around 125 μm from the center (i.e., 100 μm from the sidewall). This result was consistent with that of Bhagat et al. [1], who reported that particles migrated to about $0.4W$ from the sidewalls, where W is the half-width of the test section. The effects of Re_p and the length of the test section on the migration of rigid spheres are shown in Fig. 2.5.

When $Re_p = 0.16$, the migration of rigid spheres was not clearly observed (Fig. 2.5a). When $Re_p = 0.31$ and 0.62, inertial migration of particles toward equilibrium positions was observed. As Re_p increased, the peak of the probability density became larger. The migration of rigid spheres was not significant when $L = 0.5$ or 1.0 cm, whereas migration was apparent when $L = 1.5$ or 2.0 cm (Fig. 2.5b). These results indicate that the migration of rigid spheres occurs due to an inertial effect and that large values of Re_p and L are necessary to achieve strong migration of the spheres. These findings were consistent with those of previous studies [1,5,16]. For $Re_p = 0.16$, the migration length (L_m) was 1.3 cm. For $L = 0.5$ or 1.0 cm, the channel length was shorter than L_m ($L < L_m$). When $L = 1.5$ or 2.0 cm, the channels had adequate length ($L > L_m$). Our experimental results demonstrate that the migration length (L_m) calculated using (2.1) correctly describes the migration of rigid spheres.

2.6 Motion of Cancer Cells in a Microchannel

Next, the migration of cancer cells was compared with that of rigid spheres. Figure 2.6 shows the probability density of the width position of cancer cells upstream and downstream, with $Re_p = 0.62$. Like the rigid spheres, cancer cells displayed a relatively homogeneous probability density upstream, whereas a large peak, around 115 μm from the center (i.e., 110 μm from the wall), was observed downstream. Compared with the rigid spheres, the maximum probability density of the cancer cells was not as high and the probability density function slightly blunter.

The effects of Re_p and L on the probability density of cancer cells are shown in Fig. 2.7. The peak in the probability density increased with Re_p (Fig. 2.7a).

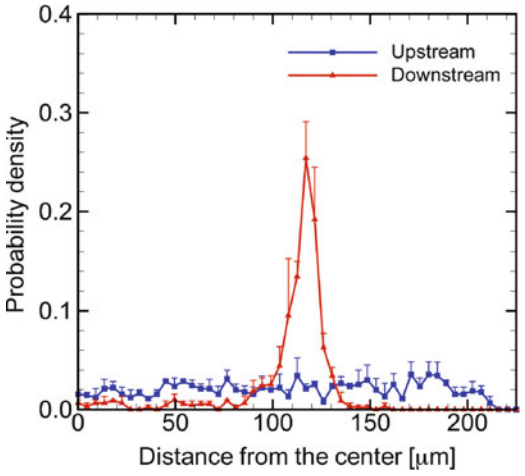

Fig. 2.6 Probability density of the width position of cancer cells at the upstream and the downstream of the test section with $Re_p = 0.62$. *Error bars* indicate standard deviations. The sidewall is located 225 μm from the center [22]

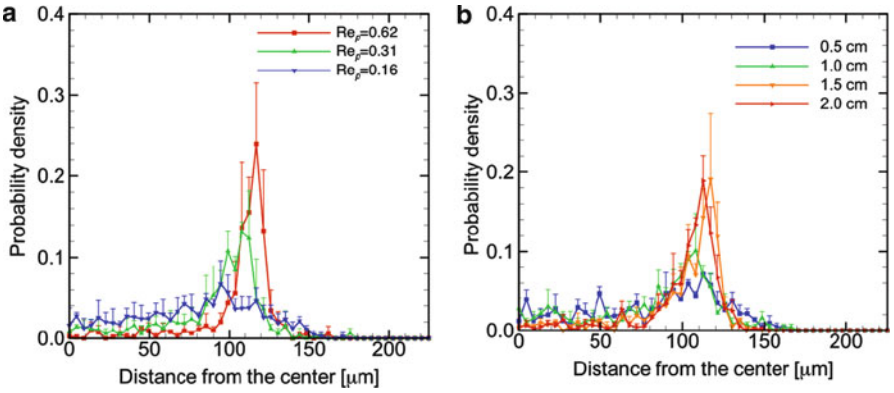

Fig. 2.7 Probability density of the width position of cancer cells at the downstream of the test section: (**a**) effect of particle Reynolds number Re_p ($L = 1.0$ cm); and (**b**) effect of the channel length L ($Re_p = 0.31$). *Error bars* indicate standard deviations [22]

For $Re_p = 0.16$, cancer cell migration was not clearly observed, as for rigid spheres (*cf.* Fig. 2.5a). For $L = 1.5$ and 2.0 cm (Fig. 2.7b), obvious migration of cancer cells was seen. These basic tendencies were the same for the rigid spheres and cancer cells.

To quantify the differences in migration properties between the rigid spheres and cancer cells, we normalized the experimental results using the migration length L_m (2.2). To quantify the migration strength, the maximum probability densities of six sections, $PD_{6,\,max}$, were calculated using the following equation:

$$PD_{6,max} = \left[\sum_{i}^{i+5} P_i\right]_{max}, \quad (i = 1 - 45) \tag{2.3}$$

where max indicates the maximum value. A large value of $PD_{6,\,max}$ indicates that large numbers of rigid spheres or cancer cells were focused in a narrow band in the width direction.

Figure 2.8 shows the correlation between L/L_m and $PD_{6,\,max}$. All of the results are plotted in the figure, covering the experimental conditions $Re_p = 0.16$–0.62 and $L = 0.5$–2.0 cm. The results differed markedly between the rigid spheres and cancer cells; the cancer cells required a greater channel length than the rigid spheres to reach the equilibrium state.

Two possible factors might have affected the migration length of cancer cells as compared with rigid spheres: their deformability and their variation in size.

Firstly, to estimate the effect of cell deformability, we introduced the capillary number, defined as $Ca = \mu\dot{\gamma}/E$, where E is Young's modulus. At a large capillary number, cells undergo marked deformation owing to high shear stress, whereas when Ca is small, cells maintain their original shape. Young's modulus for typical breast cancer cells is about 10^2 Pa [13,20], and the fluid viscosity is of the order of 10^{-3} Pa s.

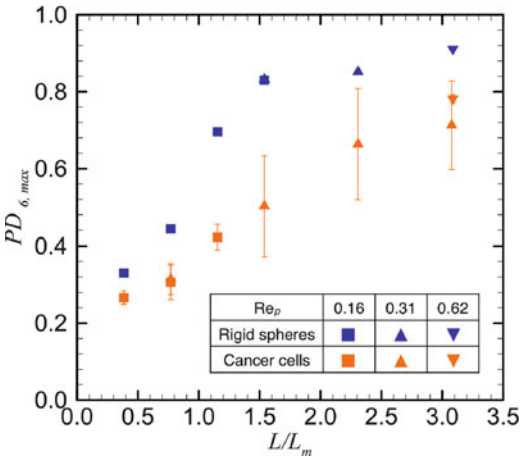

Fig. 2.8 Correlations between $PD_{6,max}$, defined by (2.3), and the normalized channel length L/L_m. The figure contains all experimental data under the conditions of $Re_p = 0.16$–0.62 and $L = 0.5$–2.0 cm. *Error bars* indicate standard deviations [22]

Consequently, Ca becomes greater than unity only when the shear rate $\dot{\gamma}$ exceeds $10^5\ s^{-1}$. In the present study, the average $\dot{\gamma}$ at the highest flow rate ($Re_p = 0.62$) was about $1.2 \times 10^4\ s^{-1}$. Therefore, the effect of cell deformability can be neglected. This was confirmed by the overlapping results of $PD_{6,max}$ obtained for different values of Re_p, which are plotted on a single curve in Fig. 2.8.

The other factor that might have affected the migration length of cancer cells compared with rigid spheres is the size variation of the cancer cells. The migration length L_m, given by (2.1), is proportional to a^{-3}, where a is the particle radius. Consequently, a small variation in cancer cell size results in a large difference in migration length. For example, the migration length of a cancer cell with radius a_0 is double that of a cancer cell with radius $1.26a_0$. The diameter distribution of cancer cells, measured using a cell counter (Vi-CELL XR cell viability analyzer; Beckman Coulter, Brea, CA), showed that the average cell diameter was about 15 μm, with a standard deviation of ~4.3 μm. In general, the size distribution of cancer cells can be expressed by the Gaussian profile of the probability density function (PDF) as

$$\mathrm{PDF}(d) = \frac{1}{\sqrt{2\pi}\sigma} \exp\left(-\frac{(d-d_0)^2}{2\sigma^2}\right), \tag{2.4}$$

where d is the diameter, d_0 is the average diameter, and σ is the standard deviation. The cumulative distribution function (CDF) in this case is

$$\mathrm{CDF}(d) = \frac{1}{2}\left[1 + \mathrm{erf}\left(\frac{d-d_0}{\sqrt{2\sigma^2}}\right)\right] \tag{2.5}$$

When $d = d_0$, CDF = 0.5. Therefore, half of the cancer cells have a migration length L_m greater than that of the rigid spheres. By substituting $d_0 = 15$ μm and $\sigma = 4.3$ μm into (2.5), it can be shown that for 18% of the cancer cells, the migration length is more than double that of the rigid spheres.

2.7 Conclusion

In this chapter we introduce our recent study of inertial migration of cancer cells in a microchannel [22]. The basic mechanism of inertial migration, fabrication of a PDMS microchannel, and the cancer cell preparation are all described. The inertial migration of both rigid spheres and cancer cells was convincingly observed in the microchannel. The migration of cancer cells in a dilute suspension was not as strong as that of rigid spheres, and the channel length required for cancer cell migration was roughly double that for the rigid spheres. The low efficiency of cell migration was attributable mainly to the size variation of the cancer cells. These results have important implications for the design of a microfluidic device for separating targeted cells from other cells.

Acknowledgments This study was supported by Grants-in-Aid for Scientific Research (S) from the Japan Society for the Promotion of Science. We also acknowledge support from the 2007 Global COE Program "Global Nano-Biomedical Engineering Education and Research Network Centre."

References

1. Bhagat AAS, Kuntaegowdanahalli SS, Papautsky I (2009) Inertial microfluidics for continuous particle filtration and extraction. Microfluid Nanofluid 7:217–226
2. Bhagat AAS, Bow H, Hou HW et al (2010) Microfluidics for cell separation. Med Biol Eng Comput 48:999–1014
3. Budd GT, Cristofanilli M, Ellis MJ et al (2006) Circulating tumor cells versus imaging-predicting overall survival in metastatic breast cancer. Clin Cancer Res 12:6403–6409
4. Carlo DD, Edd JF, Irimia D et al (2008) Equilibrium separation and filtration of particles using differential inertial focusing. Anal Chem 80:2204–2211
5. Carlo DD (2009) Inertial microfluidics. Lab Chip 9:3038–3046
6. Cristofanilli M, Budd GT, Ellis MJ et al (2004) Circulating tumor cells, disease progression, and survival in metastatic breast cancer. N Engl J Med 351:781–791
7. Cristofanilli M, Hayes DF, Budd GT et al (2005) Circulating tumor cells: a novel prognostic factor for newly diagnosed metastatic breast cancer. J Clin Oncol 23:1420–1430
8. Fujiwara H, Ishikawa T, Lima R et al (2009) Red blood cell motions in high-hematocrit blood flowing through a stenosed microchannel. J Biomech 42:838–843
9. Hur SC, Tse HTK, Carlo DD (2010) Sheathless inertial cell ordering for extreme throughput flow cytometry. Lab Chip 10:274–280

10. Ishikawa T, Fujiwara H, Matsuki N et al (2011) Asymmetry of blood flow and cancer cell adhesion in a microchannel with symmetric bifurcation and confluence. Biomed Microdevices 13:159–167
11. Jain A, Munn LL (2011) Biomimetic postcapillary expansions for enhancing rare blood cell separation on a microfluidic chip. Lab Chip 11:2941–2947
12. Kuntaegowadanahalli SS, Bhagat AAS, Kumar G et al (2009) Inertial microfluidics for continuous particle separation in spiral microchannels. Lab Chip 9:2973–2980
13. Lee GYH, Lim CT (2007) Biomechanics approaches to studying human disease. Trends Biotechnol 25:111–118
14. Matas JP, Morris JF, Guazzelli E (2004) Inertial migration of rigid spherical particles in Poiseuille flow. J Fluid Mech 515:171–195
15. Matas JP, Morris JF, Guazzelli E (2009) Lateral force on a rigid sphere in large-inertia laminar pipe flow. J Fluid Mech 621:59–67
16. Park JS, Song SH, Jung HI (2009) Continuous focusing of microparticles using inertial lift force and vorticity via multi-orifice microfluidic channels. Lab Chip 9:939–948
17. Segre G, Silberberg A (1962) Behavior of macroscopic rigid spheres in Poiseuille flow. Part 2. Experimental results and interpretation. J Fluid Mech 14:136–157
18. Sethu P, Sin A, Toner M (2006) Microfluidic diffusive filter for apheresis (leukopheresis). Lab Chip 6:83–89
19. Shevkoplyas SS, Yoshida T, Munn LL et al (2005) Biomimetic autoseparation of leukocytes from whole blood in a microfluidic device. Anal Chem 77:933–937
20. Suresh S (2007) Biomechanics and biophysics of cancer cells. Acta Mater 55:3989–4014
21. Tan SJ, Yobas L, Lee GYH et al (2009) Microdevice for the isolation and enumeration of cancer cells from blood. Biomed Microdevices 11:883–892
22. Tanaka T, Ishikawa T, Numayama-Tsuruta K et al (2011) Inertial migration of cancer cells in blood flow in microchannels. Biomed Microdevices. doi:10.1007/s10544-011-9582-y
23. Yamada M, Kano K, Tsuda Y et al (2007) Microfluidic devices for size-dependent separation of liver cells. Biomed Microdevices 9:637–645
24. Zheng S, Liu JQ, Tai YC (2008) Streamline-based microfluidic devices for erythrocytes and leukocytes separation. J Microelectromech Syst 17:1029–1038